



Amorphous TiO_2 ultrathin nanosheet for stable high-rate lithium storage

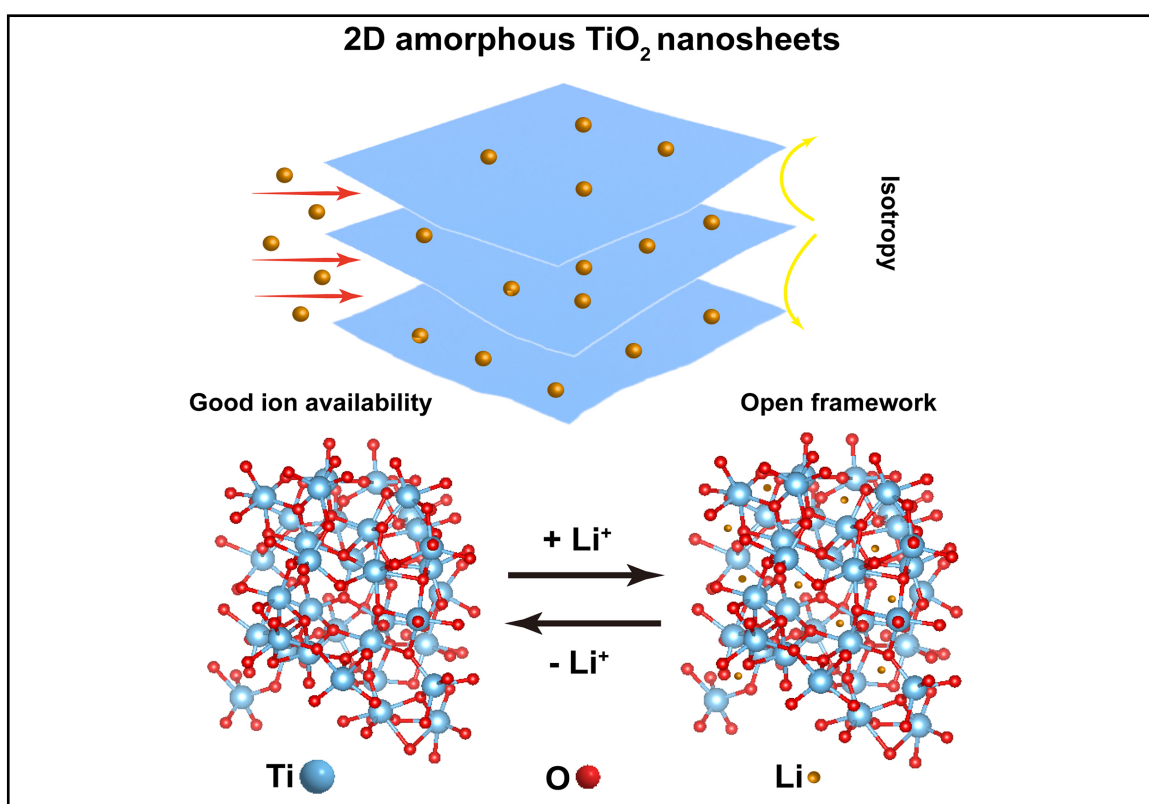
Zhongda Chen, Wenqi Zhan, Zhihao Liu, Hang Wang, Liang Wu, Zhixin Sun, and Min Zhou 

Hefei National Research Center for Physical Sciences at the Microscale, University of Science and Technology of China, Hefei 230026, China

 Correspondence: Min Zhou, E-mail: mzchem@ustc.edu.cn

© 2023 The Author(s). This is an open access article under the CC BY-NC-ND 4.0 license (<http://creativecommons.org/licenses/by-nc-nd/4.0/>).

Graphical abstract




Titanium dioxide anode with enhanced lithium storage by amorphization.


Public summary

- The isotropic amorphous titanium dioxide allows for the accommodation of the strain of ion insertion along multiple directions, reducing the damage caused by volume expansion and contraction.
- Two-dimensional nanosheet structure with large surface area ensures the effective infiltration of electrolyte. The larger specific surface area can provide more active sites, which is conducive to enhancing the contribution of interfacial capacitance.
- Compared with other TiO_2 anodes, amorphous TiO_2 anode exhibits excellent specific capacities and high-rate performance. Even at current density as high as $6 \text{ A} \cdot \text{g}^{-1}$, a specific capacity of about $160 \text{ mA} \cdot \text{h} \cdot \text{g}^{-1}$ can be obtained after 1000 cycles.

Amorphous TiO₂ ultrathin nanosheet for stable high-rate lithium storage

Zhongda Chen, Wenqi Zhan, Zhihao Liu, Hang Wang, Liang Wu, Zhixin Sun, and Min Zhou 

Hefei National Research Center for Physical Sciences at the Microscale, University of Science and Technology of China, Hefei 230026, China

 Correspondence: Min Zhou, E-mail: mzchem@ustc.edu.cn

© 2023 The Author(s). This is an open access article under the CC BY-NC-ND 4.0 license (<http://creativecommons.org/licenses/by-nc-nd/4.0/>).



Cite This: *JUSTC*, 2023, 53(6): 0605 (9pp)



Read Online



Supporting Information

Abstract: The use of intercalation-type metal oxides as anode materials in rechargeable lithium-ion batteries is appealing due to their reduced risk of Li plating at low voltages. However, their implementation for fast-charging applications is limited by their lower energy and power density, as well as cycling instability. Herein, we present an amorphous TiO₂ nanosheet that exhibits exceptional cycling stability with a high capacity of 231 mA·h·g⁻¹ after 200 cycles at 500 mA·g⁻¹ and 156.7 mA·h·g⁻¹ after 1000 cycles at a high current density of 6 A·g⁻¹. We attribute the enhanced rate performance to the amorphous nature with high isotropy, which facilitates low energy migration paths and ion availability and can accommodate large changes in volume. This work suggests that amorphization represents a promising strategy for developing unconventional metal oxide electrode materials with high-rate performance.

Keywords: amorphization; TiO₂; ultrathin nanosheet; lithium-ion batteries; template-induced fabrication

CLC number: TB383

Document code: A

1 Introduction

The escalating demands for electronic energy storage are attributed to the growing market requirements. Lithium-ion battery (LIB) technology has emerged as the preeminent power source for many modern electronic devices and, as such, has revolutionized the way in which electrical energy is utilized in our daily lives. The attainment of new performance benchmarks in energy storage necessitates the development of pioneering battery materials^[1,2]. Naturally, abundant TiO₂ stands out as an anode material due to its various merits, such as reversible redox pair (Ti³⁺/Ti⁴⁺) with a theoretical specific capacity of 335 mA·h·g⁻¹, low volumetric variation during the (de)intercalation, long-term cycling stability, low cost, and environmental friendliness^[3,4]. However, one major obstacle for TiO₂ is its limited capacity at high rates. Several effective approaches have been taken to enhance its rate performance, including morphology design, defect engineering, surface coating, and composites with conductive materials^[5]. Parallel to these efforts on crystalline materials, there is a rising interest in amorphous materials for fast charge/discharge^[6–10] because amorphous materials with isotropic characteristics can create percolation pathways to facilitate ionic storage and migration by activating open diffusion channels, a large surface area and good wettability with electrolytes, and a strong ion affinity to improve the interface capacitive-like capacities^[11,12]. Hence, amorphous TiO₂ is promising to face the challenges of low ion adsorption and further optimize the rate performance^[13–15].

Nanosheets belong to a class of materials that share structural similarities with graphene, possessing 2D architectures.

These graphene-like nanosheets possess atomic-level thickness, impressive mechanical strength, and tunable electronic properties, making them distinct due to their molecular thickness and large lateral dimensions that differ by 2–5 orders of magnitude. Due to their 2D nature, nanosheets boast a significantly higher specific surface area than their 3D counterparts and may experience physical phenomena resulting from quantum confinement in one principal direction. Consequently, the development of two-dimensional (2D) nanomaterials has attracted attention for their potential use in lithium-ion batteries. This design maximizes the advantages of the material's inherent structure, promoting efficient electron transport and ion diffusion. Additionally, it helps to optimize the electrode matrix by creating continuous conductive paths, ultimately enhancing its capacities and stability.

In this work, amorphous TiO₂ nanosheets have been realized by a salt-template method, delivering excellent long-term and fast lithium storage. Achieving a high reversible lithium-storage capacity of 139 mA·h·g⁻¹ is feasible at a current density of 10 A·g⁻¹, and maintaining a high capacity of approximately 156.7 mA·h·g⁻¹ even after 1000 cycles is also possible at a current density as high as 6 A·g⁻¹. Such amorphous TiO₂ nanosheets with satisfactory rate capacities highlight the importance of amorphization for electrode design at the atomic level.

2 Materials and methods

2.1 Materials and fabrication

Ten microliters of tetrabutyl titanate (TBOT) was rapidly added to 5 mL of anhydrous ethanol and vigorously stirred by

ultrasonication for 5 min to obtain a uniform faint yellow solution. Then, the solution was poured into 20 g potassium chloride (KCl) and stirred vigorously for 10 min to obtain an even mix. The mixture was then dried at 70 °C to remove excess solvent and left in a high humidity environment for 12 h. Afterwards, the mixture was heated in a muffle furnace to 350 °C at a rate of 3 °C·min⁻¹ in an air atmosphere and maintained at this temperature for 1 h. Finally, the obtained product was centrifugally washed in deionized water several times and then filtered to remove the salt template. The amorphous nanosheets were dried and collected. The synthesis of crystalline materials was basically the same, with the only difference being that the annealing temperature was changed to 500 °C.

2.2 Characterization

Scanning electron microscopy (SEM) characterization was performed by an FEI Quanta250 FEG microscope. Transmission electron microscopy (TEM) analysis was performed by a JEM-2100 Plus microscope with a 200 kV accelerating voltage. The thickness of the nanosheets was measured by atomic force microscopy (AFM, Dimension Icon, Bruker). X-ray diffraction tests with Cu K α radiation ($\lambda = 1.5406$ Å) were performed on a Rigaku Miniflex-600 with an operating voltage of 40 kV and a current of 15 mA. Raman spectra were acquired using a 633 nm laser and detected by a LabRAM HR spectrometer. X-ray photoelectron spectroscopy (XPS, Escalab 250, Thermo Fisher Scientific) was used to detect the elemental chemical status on the surface of the samples. The value of binding energy was corrected by the value of the C1s peak position of contaminant carbon at 284.80 eV.

2.3 Electrochemical measurements

The working electrodes were prepared by grinding and dispersing TiO₂ (60 wt%), Super P (10 wt%), CNTs (10 wt%) and polyvinylidene fluoride (10 wt%) into N-methyl-2-pyrrolidone (NMP). The obtained slurry was evenly coated on the smooth side of the copper foil with a thickness of 15 μ m and then vacuum-dried at 80 °C for 12 h. Then, the foil was cut into 12 mm rounds with a loading mass of active materials of approximately 0.6 mg·cm⁻² \pm 0.1 mg·cm⁻². Celgard 2400 served as the separator, a metal lithium sheet served as the counter electrode, and 1 mol/L LiPF₆ dissolved in ethylene carbonate and diethyl carbonate (v : v=1 : 1) served as the electrolyte. All the electrochemical properties were tested with typical CR2032 coin half cells. CV, GITT, and EIS measurements were measured by a BioLogic electrochemical workstation between 0.01 and 3.0 V with scan rates ranging from 0.1 to 5.0 mV·s⁻¹.

3 Results and discussion

Amorphous TiO₂ nanosheets were fabricated through a salt-template approach, as shown in Fig. 1a. Here, KCl was chosen as the template due to its relatively high interfacial force with TiO₂, so amorphous TiO₂ can be obtained within wider temperature ranges. After annealing at 350 °C, micrometer-scale nanosheets can be observed in representative SEM and TEM images in Fig. 1b–d. The near-transparent appearance indicates the ultrathin feature. The comprehensive

two-dimensional conformability provides additional confirmation of the complete topological transformation from the salt template. Regarding the phase of the nanosheets, the amorphous nature is evident from the featureless selected area electron diffraction (SAED) pattern of the entire nanosheet in the inset of Fig. 1e, and this conclusion is further strengthened by the high-resolution TEM (HRTEM) image in Fig. 1e, where no noticeable lattice fringe is observed. We will refer to this sample as a-TiO₂ henceforth in the subsequent text. With an increase in annealing temperature to 500 °C, the morphological features remain almost unchanged. However, the nanosheets become almost fully crystallized with a rough surface represented as c-TiO₂ in Fig. 1f. Further evidence is provided by the FFT pattern of the entire nanosheet in the inset of Fig. 1g. The HRTEM image, with clear lattice fringes assigned to the (101) and (011) facets of anatase TiO₂, proves that the crystalline nanosheet comprises small TiO₂ nanoparticles with numerous grain boundaries^[16]. It is noteworthy that no grain boundary can be observed in amorphous nanosheets, which could positively impact ion migration during electrochemical cycling. In reference to the nanosheet dimensions, thickness measurements were successfully obtained for TiO₂ nanosheets via atomic force microscopy (AFM), as detailed in Fig. S1 (Supporting information). The findings indicated that the thicknesses of amorphous TiO₂ (a-TiO₂) and crystalline TiO₂ (c-TiO₂) were approximately 5.14 nm and 5.23 nm, respectively, demonstrating their ultrathin characteristics.

The amorphous nature of a-TiO₂ is further verified by the XRD pattern and Raman spectra. X-ray diffraction (XRD) is a technique widely recognized for providing insight into the long-range order of materials. As such, it can provide valuable average structural information over long ranges. The absence of any diffraction peaks in the XRD pattern (Fig. 2a) of a-TiO₂ confirms its amorphous nature, as opposed to the strong diffraction peaks observed in the XRD pattern of c-TiO₂ assigned to anatase TiO₂ (141/amd, JCPDF 21-1272). Additionally, since Raman scattering is a local probe that is highly sensitive to the local symmetry, the lack of Raman response in a-TiO₂ in comparison to the spectra of c-TiO₂, where anatase TiO₂ Raman modes were detected in Fig. 2b, strongly suggests a loss of long-range orderliness in the atomic arrangement, substantiating the amorphous nature of a-TiO₂. The chemical states of a-TiO₂ and c-TiO₂ were analyzed using XPS measurements. The two characteristic peaks in Fig. 2c reveal that Ti existed mainly as Ti⁴⁺ in the lattice in a-TiO₂ and c-TiO₂ rather than Ti³⁺ or Ti⁰. Furthermore, the increased Ti 2p_{3/2} (Ti-O) and O 1s binding energies observed for a-TiO₂ compared to c-TiO₂ suggest that the oxygen-rich compositions led to an increase in the chemical valence of Ti and O due to the screening effect in Ti 2p of a-TiO₂^[17]. The quantification analysis indicates that a-TiO₂ (O:Ti = 2.536) exhibits a higher oxygen content than c-TiO₂ (O:Ti = 2.368). This phenomenon can be rationalized by an increase in oxygen-rich constituents present in the a-TiO₂ phase. Definitely, the elevated oxygen concentration in a-TiO₂ significantly impacts the interplay between O and the Ti⁴⁺ center, leading to a greater extent of O atoms surrounding Ti⁴⁺ when compared to c-TiO₂. This interaction results in a slight elevation in the

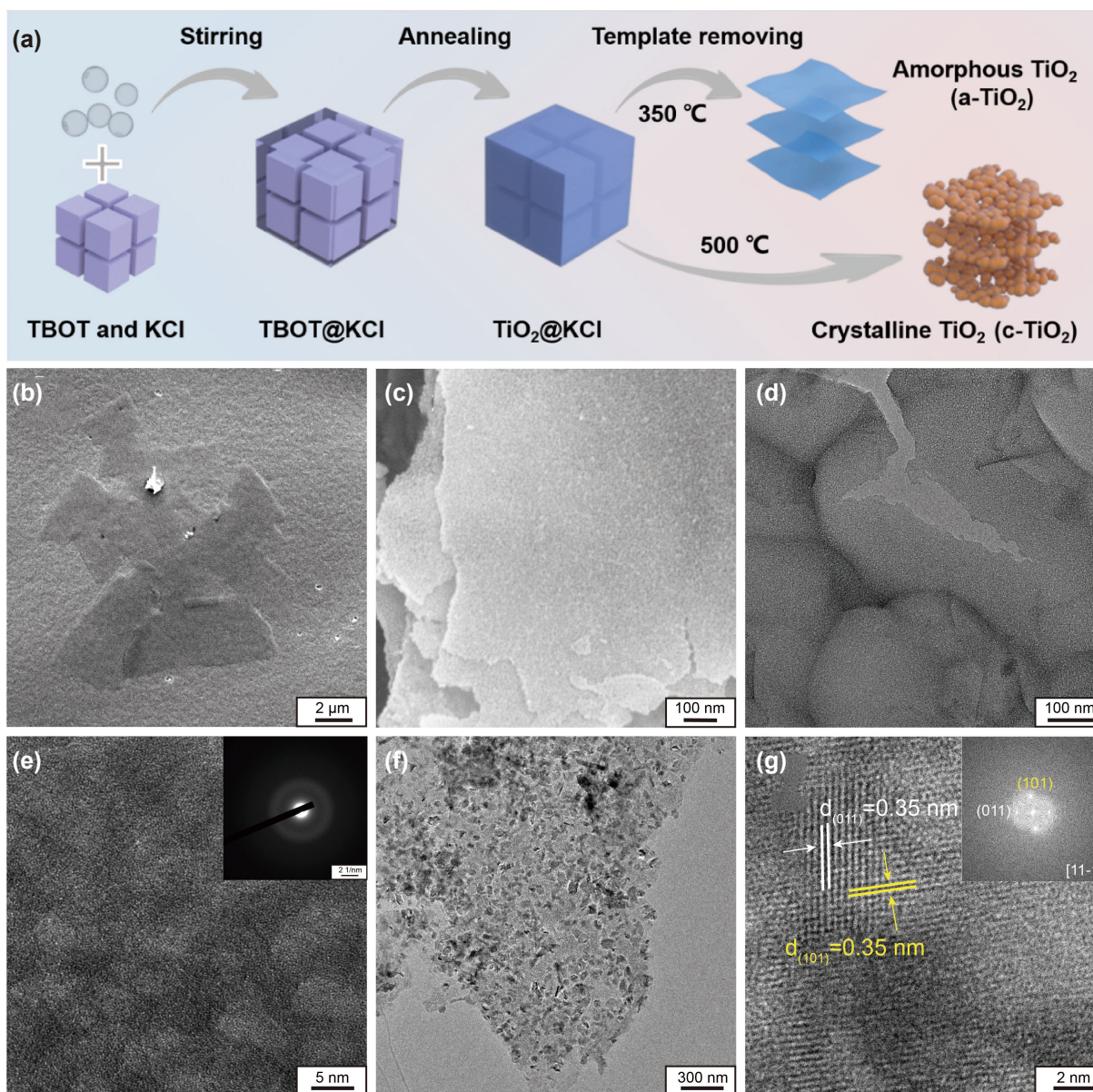


Fig. 1. (a) Schematic illustration of the synthesis of a-TiO₂ and c-TiO₂. (b) SEM image of a-TiO₂. (c) SEM image of a-TiO₂ for details. (d) TEM image of a-TiO₂. (e) HRTEM image of a-TiO₂ with the inset of SAED pattern. (f) TEM image of c-TiO₂. (g) HRTEM image of c-TiO₂ with the inset of the SAED pattern.

chemical valence of O in a-TiO₂. Correspondingly, the O 1s peak in a-TiO₂ experiences a minor shift toward higher binding energies.

To quantify the lithium storage ability, two-electrode coin cells were employed with TiO₂ anodes, as diagramed in Fig. 3a. Cyclic voltammetry (CV) was first recorded to elucidate the redox processes in amorphous and crystalline host matrices with different long-term ordering. The CV curves of the 3rd cycle at a sweep rate of 0.1 mV·s⁻¹ in the potential range of 0.01–3.0 V (vs. Li/Li⁺) are shown in Fig. 3b. The curve of c-TiO₂ displays a redox couple at 2.13 V (anodic) and 1.70 V (cathodic), indicating the reversible insertion/extraction of lithium. On the other hand, the curve of a-TiO₂ shows no peaks over the entire potential range. This suggests that there is a wide distribution of redox events associated with the broad energy dispersion of lithiation sites in a-TiO₂. The

intercalation reaction within TiO₂ is a promising approach for the development of stable lithium-ion batteries. The overall reaction to describe the electrochemical process of lithium intercalation/extraction into TiO₂ can be exhibited as $x\text{Li}^+ + x\text{e}^- + \text{TiO}_2 \rightarrow \text{Li}_x\text{TiO}_2$. The observed difference in electrochemical behavior between c-TiO₂ and a-TiO₂ could be attributed to their crystal structures and surface state. c-TiO₂ has a well-defined crystal structure with ordered channels that allow for lithium insertion/extraction, whereas a-TiO₂ has an amorphous structure with more types of open channels that endow lithium diffusion and result in a lower capacity and efficiency in lithium-ion battery applications. Additional studies are needed to further understand the impact of long-term orderliness on the electrochemical performance of TiO₂-based anodes. More information can be revealed from the voltage profiles to illustrate the electrochemistry of (de-)lithiation in

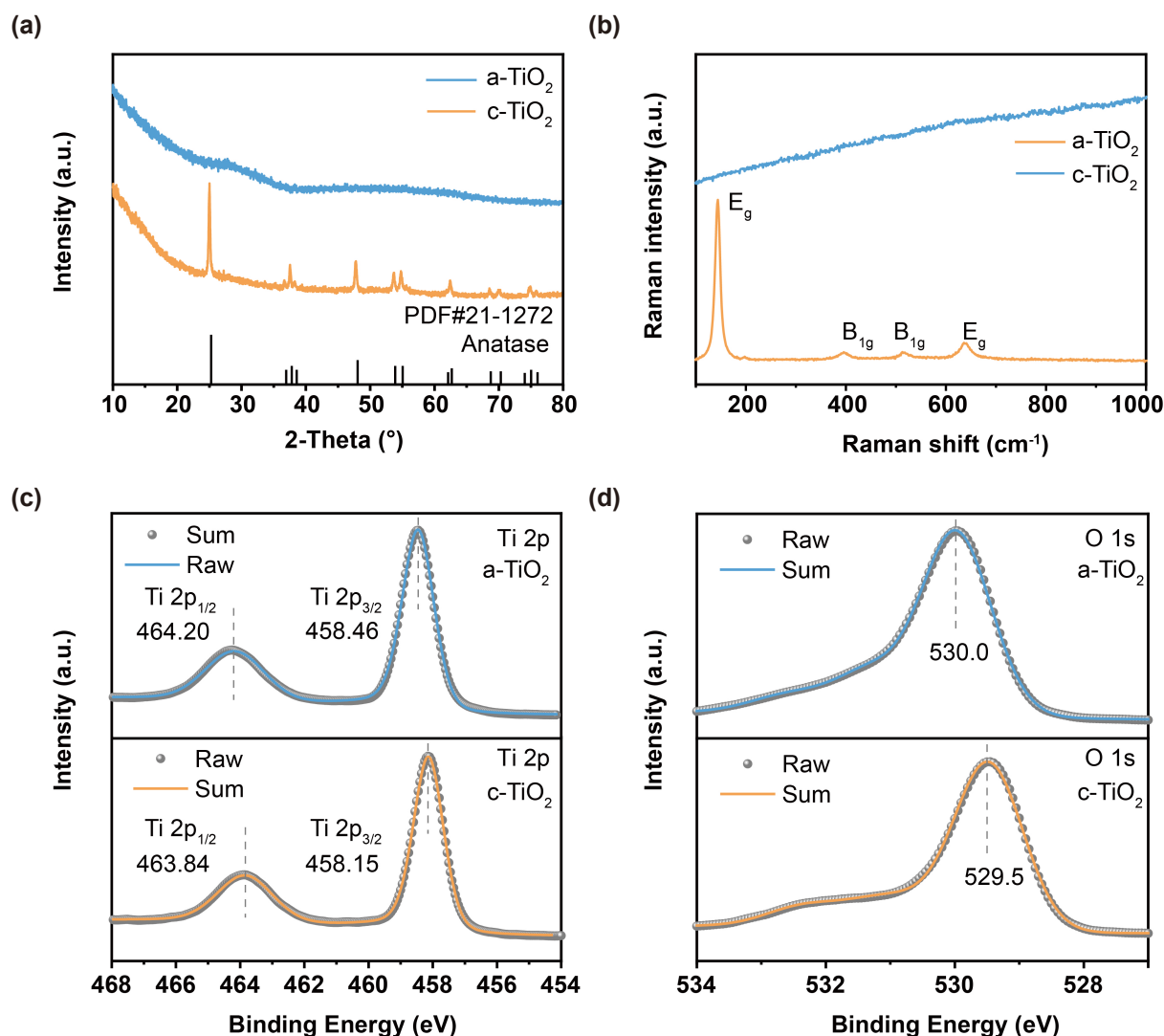


Fig. 2. Detailed characterizations of a-TiO₂ and c-TiO₂. (a) XRD patterns, (b) Raman spectra, (c) XPS Ti 2p spectra of a-TiO₂ and c-TiO₂, and (d) XPS O 1s spectra of a-TiO₂ and c-TiO₂.

the host. Fig. 3c displays the discharge voltage profiles of a-TiO₂ and c-TiO₂ during the 1st, 2nd, and 10th cycles at a current density of 50 mA·g⁻¹. By comparing the discharge profiles after different cycles, we observed that a-TiO₂ exhibits a slope feature, whereas c-TiO₂ shows a more pronounced plateau. These observations further demonstrate the redox behavior based on cyclic voltammetry analysis. Notably, the initial discharge capacity of a-TiO₂ is 1038 mA·h·g⁻¹, which decreases to 374 mA·h·g⁻¹ after 10 cycles. In contrast, c-TiO₂ shows specific capacities of 649 and 317 mA·h·g⁻¹. The lithium storage capacity of a-TiO₂ is comparable to the theoretical value (335 mA·h·g⁻¹), emphasizing its outstanding ability to store lithium. These extra capacities are mainly derived from the contribution of interface capacitive-like storage, which typically occurs within seconds and minutes^[18]. Therefore, increasing the interface capacitive-like storage in a-TiO₂ is anticipated to effectively balance high capacity and high rate performance.

To examine the feasibility of high-power applications, the comparison of rate performance in Fig. 3d further confirms

the evolution of the specific capacities upon cycling. The capacities of a-TiO₂ are 374.5, 340.86, 312.4, 274.4, 242.4, 210.6, 179.5, 163.5 and 150.5 mA·h·g⁻¹ at current rates of 0.05, 0.1, 0.2, 0.5, 1, 2, 4, 6 and 8 A·g⁻¹, respectively. As expected, even when subjected to a high current density of 10 A·g⁻¹, the specific capacity of a-TiO₂ achieved was approximately 139 mA·h·g⁻¹, which is 5.18 times greater than that of c-TiO₂. Such excellent rate performance stands out among titanium dioxide electrodes for lithium-ion batteries (Table S1 and Fig. S3). It is important to note that at 50 mA·h·g⁻¹, the ratio drops to only 1.18, indicating that the specific capacities of the c-TiO₂ anode decrease rapidly as the rate increases. Following cycling at high rates, a-TiO₂ demonstrates a specific capacity of approximately 380 mA·h·g⁻¹ after returning to a current density of 50 mA·g⁻¹. In addition to its exceptional capacity at high rates, a-TiO₂ exhibits an impressive retention of 97% from the second cycle to the 200th cycle at 500 mA·g⁻¹ (Fig. 3e). Moreover, even after 1000 cycles at 6 A·g⁻¹ (Fig. 3f), a-TiO₂ can still maintain a capacity of approximately 156.7 mA·h·g⁻¹ with an ~85% capacity retention ratio, which

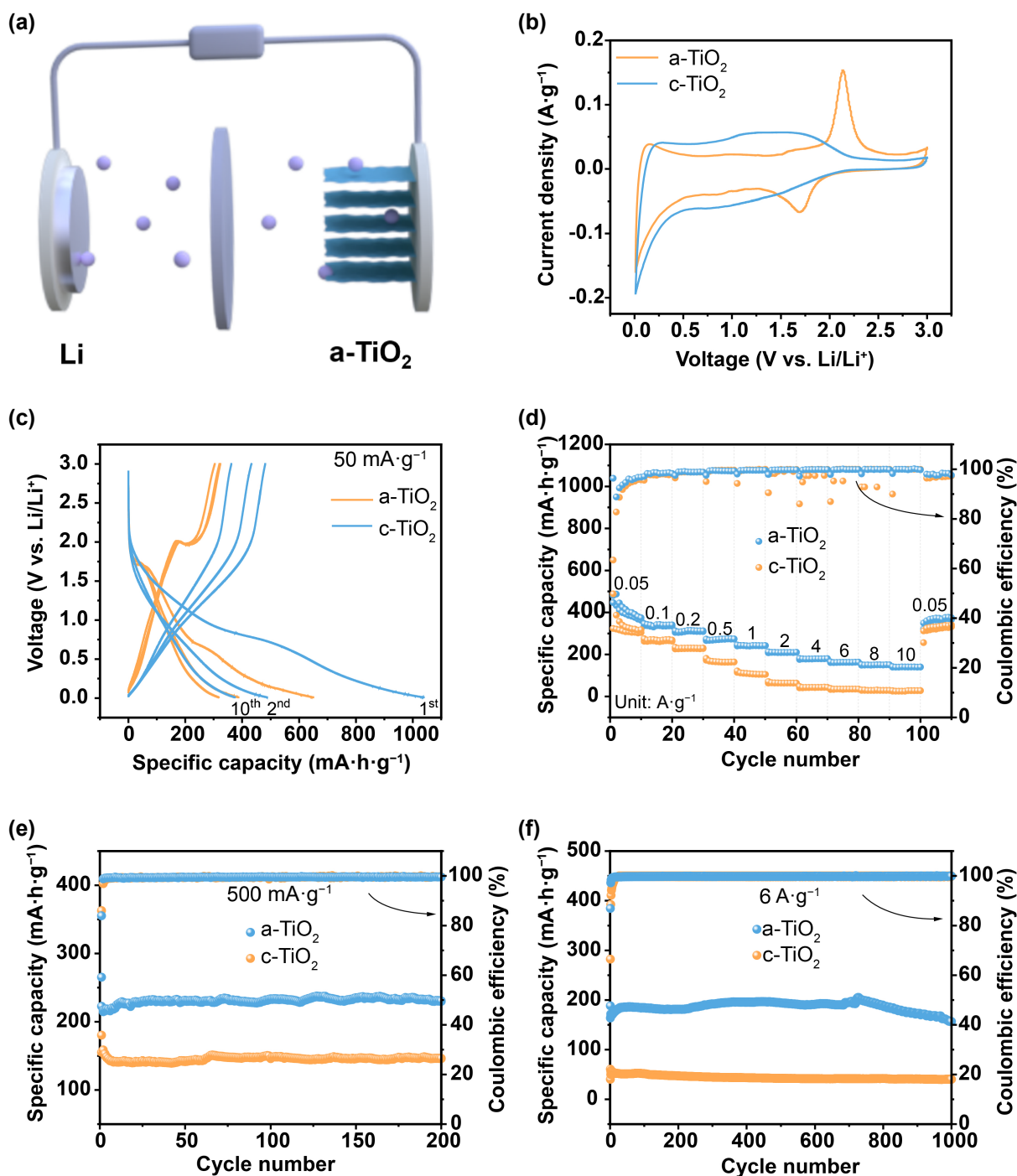


Fig. 3. (a) Detailed schemes of TiO₂-based lithium-ion batteries. (b) CV curves at 0.1 mV·s⁻¹. (c) Galvanostatic discharge/charge profiles of the 1st, 2nd and 10th cycles at 50 mA·g⁻¹. (d) Rate performance. (e) Cycling performances of the a-TiO₂ and c-TiO₂ electrodes at 500 mA·g⁻¹. (f) Cycling performances at 6 A·g⁻¹.

is almost 3.87 times higher than that of c-TiO₂. Our investigation into the cycling and rate performance of a-TiO₂ and c-TiO₂ has led us to conclude that a-TiO₂ exhibits feasible, stable, and reversible high-rate storage capabilities for lithium. This makes a-TiO₂ an excellent option for high-rate lithium storage applications. We have also noted that the extent of atomic order over a long range significantly affects the LIB performance.

This observation prompts us to consider the relationship between the amorphous nature and their performance in LIBs, particularly under high-rate conditions. Since the active materials are identical and the accommodation of Li ions should, in theory, be the same for both TiO₂ materials, we set out to identify the underlying kinetic factors that may contribute to this observed trend. To achieve this, we employed CV analysis, a powerful technique for elucidating the electrochemical

kinetics of an electrode in relation to Li⁺. By examining the current response to applied sweep rates, we can determine whether the redox reaction is diffusion-controlled^[9]. Thus, we conducted CV experiments of a-TiO₂ and c-TiO₂ at various

scan rates ranging from 0.1 to 5.0 mV·s⁻¹, as shown in Fig. 4a, b. The redox pairs that we have identified closely match the potentials of the reversible Ti⁴⁺/Ti³⁺ redox, which is consistent with the conclusions drawn from Fig. 3b. It is well known

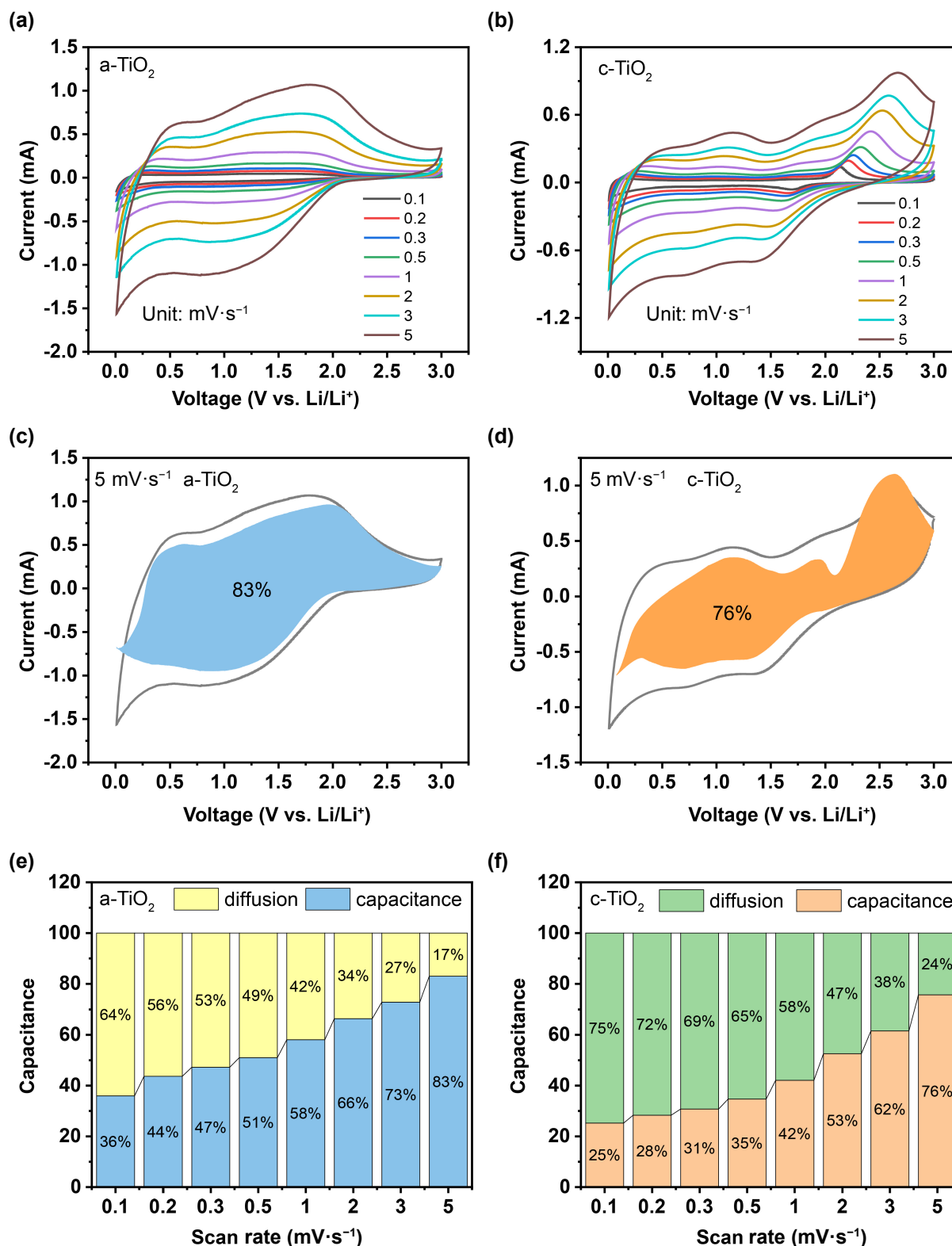


Fig. 4. (a–b) CV curves of the a-TiO₂ and c-TiO₂ electrodes at various scan rates in the range of 0.1 to 5.0 mV·s⁻¹. (c–d) The pseudocapacitive contribution at different scan rates. (e–f) CV curves with the capacitive fraction area (blue and orange regions) at a scan rate of 5.0 mV·s⁻¹.

that the process of ion intercalation involves three main stages: first, solvated Li^+ diffuses within the electrolyte; second, charge-transfer reactions occur at or near the interface between active materials and the electrolyte; and last, Li -ion diffusion takes place within the bulk materials. By observing the unique electrochemical behaviors during these stages, two types of contributions to lithium storage can be identified. The first type pertains to Li -ion intercalation within the bulk and is related to a diffusion-controlled mechanism.

The second type is capacitance at or near the interface. To obtain a better understanding of the storage mechanism, the current response (i) can be separated at a fixed potential into contributions from bulk Li -ion intercalation and interface capacitance. These contributions can be mathematically defined using the following equation:

$$i = k_1 v + k_2 v^{1/2}. \quad (1)$$

By incorporating adjustable constants k_1 and k_2 into this

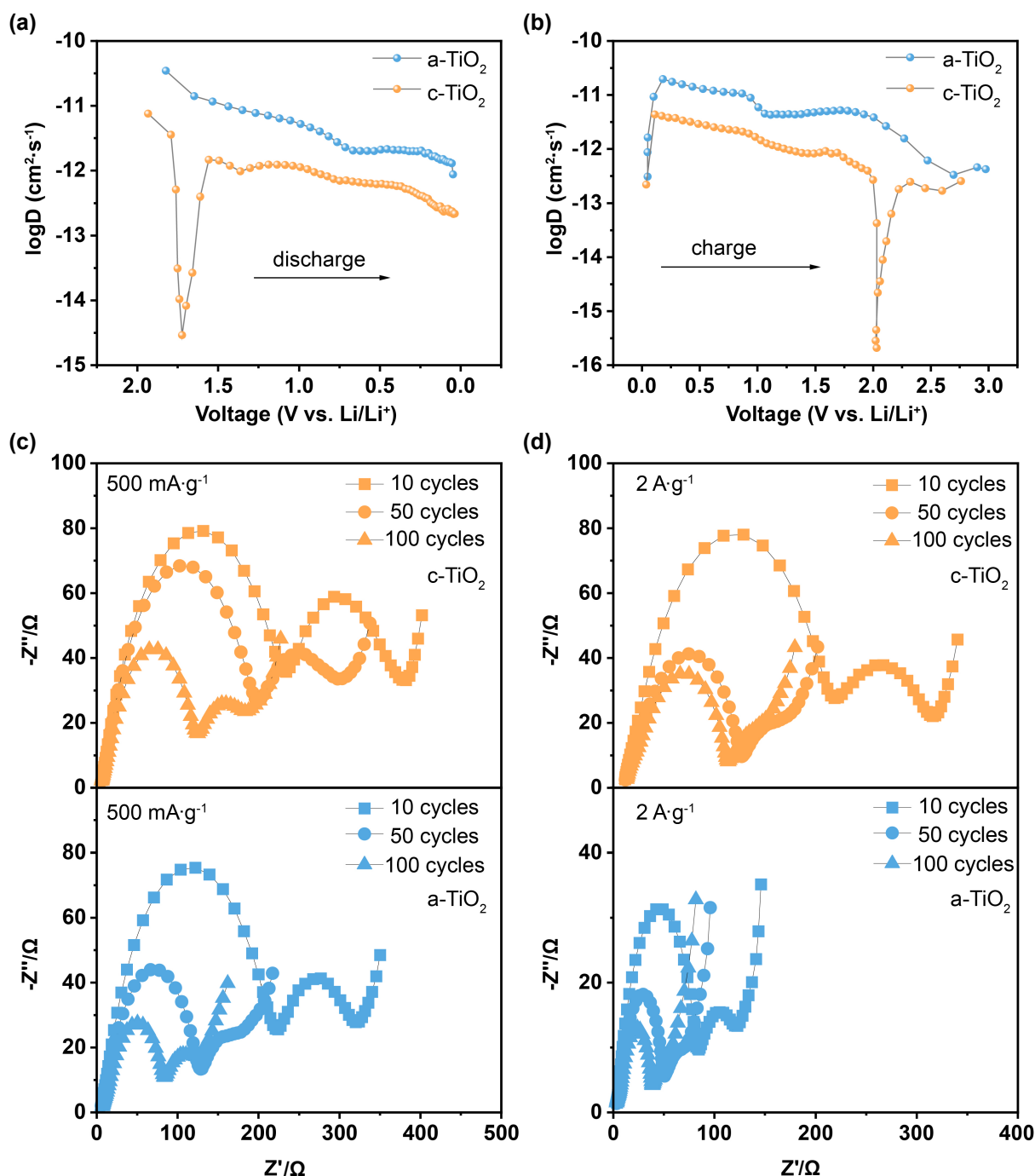


Fig. 5. (a) Li^+ diffusion coefficient of a-TiO₂ and c-TiO₂ during discharging. (b) Li^+ diffusion coefficient of a-TiO₂ and c-TiO₂ during charging. (c) Electrochemical impedance spectroscopy after 10, 50, and 100 cycles at a current density of 500 mA·g⁻¹. (d) Electrochemical impedance spectroscopy after 10, 50, and 100 cycles at a current density of 2 A·g⁻¹.

equation, we can solve for their values at each potential, which assists in separating the diffusion-controlled currents and capacitive-like currents. This is feasible because the former exhibits proportionality to v , whereas the latter exhibits proportionality to $v^{1/2}$.

The quantitative analysis presented in Fig. 4c and 4d clearly shows that the interface capacitive-like contribution improves gradually as the scan rate increases. Specifically, at a scan rate of 0.1 mV·s⁻¹, approximately 36% of the total capacity is capacitive in nature. This capacitance ratio increases to 83% with an improved scan rate of 5.0 mV·s⁻¹, while the value is only 76% for c-TiO₂. Fig. 4e and 4f portray the typical CV curves corresponding to the capacities obtained from interface capacitance-like contributions (blue and orange regions) in comparison to the total capacities when scanned at 5.0 mV·s⁻¹. After considering the same mass loading and morphology parameters, the outcomes clearly suggest that the introduction of long-term amorphization successfully improves the capacity of the interface capacitance-like lithium storage and further excellent lithium storage ability at high rates.

To investigate the electrochemical kinetic characteristics of both a-TiO₂ and c-TiO₂ electrodes, the galvanostatic intermittent titration technique (GITT) was utilized to observe the Li⁺ diffusion coefficient (D_{Li^+}). GITT data (Fig. S2) were analyzed with a current pulse duration of 10 min and an interval time of 1 h while using a current density of 50 mA·g⁻¹ during the second cycle. As depicted in Fig. 5a and 5b, the D_{Li^+} of the a-TiO₂ electrode was found to be significantly higher than that of the c-TiO₂ electrode during the process of lithium intercalation and delithiation. This led to the average D_{Li^+} of a-TiO₂ being 4.6×10^{-12} and 3.3×10^{-12} cm²·s⁻¹ during discharging and charging, respectively, which was 5.6 and 4.1 times that of c-TiO₂. Consequently, the introduction of amorphization resulted in enhanced Li⁺ diffusion kinetics and a superior rate as well as a fast-charge capability. Additionally, after 10, 50, and 100 cycles at current densities of 500 mA·g⁻¹ and 2 A·g⁻¹ (Fig. 5c and 5d), electrochemical impedance spectroscopy measurements were carried out on both a-TiO₂ and c-TiO₂ electrodes, and the results showed that a-TiO₂ had the lowest charge transfer resistance at every cycle number, demonstrating that amorphization acceleration truly enhances the kinetics of lithium ions^[20,21].

Given these analyses, our results prove that amorphization is beneficial for lithium storage at high rates. First, to facilitate ion diffusion, lithium ions hop between neighboring sites along shared edges with strong electrostatic repulsion between Li and adjacent Ti atoms. This causes a distortion in the Li-O polyhedrons, allowing Li-ion hopping between them, which changes the length of the shared edge and creates a significant energy barrier for Li-ion diffusion. This variation may result from the challenging diffusion barrier of Li ions in a long-range ordered matrix, which must adhere to crystalline symmetry requirements. A higher ratio of shortened Ti-O bonds impedes mobility and increases the difficulty of diffusion in c-TiO₂. In contrast, amorphous arrangements with high isotropy provide a more open framework for ion transport and tolerate distortion during (de)lithiation, thus facilitating Li-ion diffusion more effectively in a-TiO₂ than in

c-TiO₂. Second, the surface amorphization process creates a rough surface at the atomic level that enhances the attraction of Li ions. Additionally, the surfaces possess sufficient ion availability due to good solvent wettability and electrolyte penetration, which allows for a significant surface interface capacitive contribution. These factors combine to improve the capacities at high rates. Third, open frameworks in a-TiO₂ nanosheets have the advantage of accommodating the volume changes induced by storing lithium, which helps stabilize their long-term capacity retention. Amorphization, which optimizes ion kinetics, enables highly effective storage of lithium within the electrode matrix^[22]. This discovery offers valuable insights into the development of electrode materials that utilize the intercalation mechanism.

4 Conclusions

The development of amorphous TiO₂ ultrathin nanosheets has successfully addressed the challenge of high-rate performance for lithium-ion batteries. This type of anode exhibits significantly higher specific capacities and high-rate performance compared to other TiO₂ anodes. After 200 cycles at 500 mA·g⁻¹, the retained capacity can reach approximately 231 mA·h·g⁻¹, and even at a current density as high as 6 A·g⁻¹, a capacity of approximately 160 mA·h·g⁻¹ can be achieved with ~85% capacity retention. The high isotropy of a-TiO₂ lattices, along with an open framework, good ion availability, and large volume change accommodation, make amorphization suitable for lithium storage within the electrode matrix, particularly at high rates. Our results demonstrate the significance of optimizing kinetic factors as a prerequisite for superior electrode design at the atomic level in achieving high electrochemical performance and offer significant promise for the development of intercalation electrodes for various secondary ion batteries.

Supporting information

The supporting information for this article can be found online at <https://doi.org/10.52396/JUSTC-2023-0057>. The supporting information includes three figures and one table.

Acknowledgements

This work was supported by the National Natural Science Foundation of China (52002366, 22075263) and the Fundamental Research Funds for the Central Universities (WK2060000039). The authors wish to acknowledge the support from the USTC Center for Micro- and Nanoscale Research and Fabrication and the supercomputing system in the Supercomputing Center of USTC for helpful discussions regarding the experimental design.

Conflict of interest

The authors declare that they have no conflict of interest.

Biographies

Zhongda Chen is currently a master's student in the School of Chemistry and Materials Science, University of Science and Technology of

China. His research mainly focuses on amorphous TiO₂ in alkali metal ion batteries.

Min Zhou received her Ph.D. degree in Inorganic Chemistry from the University of Science and Technology of China. She is currently a Professor in Hefei National Research Center for Physical Sciences at the Microscale, University of Science and Technology of China. Her research mainly focuses on material geometry.

References

- [1] Li S Q, Wang K, Zhang G F, et al. Fast charging anode materials for lithium-ion batteries: Current status and perspectives. *Adv. Funct. Mater.*, **2022**, 32 (23): 2200796.
- [2] Li M, Lu J, Chen Z, et al. 30 years of lithium-ion batteries. *Adv. Mater.*, **2018**, 30 (33): 1800561.
- [3] Wang W G, Liu Y, Wu X, et al. Advances of TiO₂ as negative electrode materials for sodium-ion batteries. *Adv. Mater. Technol.*, **2018**, 3 (9): 1800004.
- [4] Zhang Y Y, Tang Y X, Li W L, et al. Nanostructured TiO₂-based anode materials for high-performance rechargeable lithium-ion batteries. *ChemNanoMat*, **2016**, 2 (8): 764–775.
- [5] Yan X D, Wang Z H, He M, et al. TiO₂ nanomaterials as anode materials for lithium-ion rechargeable batteries. *Energy Technology*, **2015**, 3 (8): 801–814.
- [6] Barnes P, Zuo Y, Dixon K, et al. Electrochemically induced amorphous-to-rock-salt phase transformation in niobium oxide electrode for Li-ion batteries. *Nat. Mater.*, **2022**, 21 (7): 795–803.
- [7] Liu Y, Ding C F, Yan X D, et al. Interface-strain-confined synthesis of amorphous TiO₂ mesoporous nanosheets with stable pseudocapacitive lithium storage. *Chem. Eng. J.*, **2021**, 420: 129894.
- [8] Zhou M, Xu Y, Wang C L, et al. Amorphous TiO₂ inverse opal anode for high-rate sodium ion batteries. *Nano Energy*, **2017**, 31: 514–524.
- [9] Zhou M, Xu Y, Xiang J X, et al. Sodium-ion batteries: Understanding the orderliness of atomic arrangement toward enhanced sodium storage. *Adv. Energy Mater.*, **2016**, 6 (23): 1600448.
- [10] Augustyn V, Simon P, Dunn B. Pseudocapacitive oxide materials for high-rate electrochemical energy storage. *Energy Environ. Sci.*, **2014**, 7 (5): 1597–1614.
- [11] Xiong H, Yildirim H, Shevchenko E V, et al. Self-improving anode for lithium-ion batteries based on amorphous to cubic phase transition in TiO₂ nanotubes. *J. Phys. Chem. C*, **2012**, 116: 3181–3187.
- [12] Gao Q, Gu M, Nie A M, et al. Direct evidence of lithium-induced atomic ordering in amorphous TiO₂ nanotubes. *Chem. Mater.*, **2014**, 26 (4): 1660–1669.
- [13] Liu Y, Ding C F, Xie P T, et al. Surface-reconstructed formation of hierarchical TiO₂ mesoporous nanosheets with fast lithium-storage capability. *Mater. Chem. Front.*, **2021**, 5 (7): 3216–3225.
- [14] Yan S H, Abhilash K P, Tang L Y, et al. Research advances of amorphous metal oxides in electrochemical energy storage and conversion. *Small*, **2019**, 15 (4): 1804371.
- [15] Deng C J, Lau M L, Ma C R, et al. A mechanistic study of mesoporous TiO₂ nanoparticle negative electrode materials with varying crystallinity for lithium ion batteries. *J. Mater. Chem. A*, **2020**, 8: 3333–3343.
- [16] Wu J X, Liu H W, Tang A W, et al. Unexpected reversible crystalline/amorphous (de)lithiation transformations enabling fast (dis)charge of high-capacity anatase mesocrystal anode. *Nano Energy*, **2022**, 102: 107715.
- [17] Qi Y, Zeng X Q, Xiao L P, et al. An invisible hand: Hydrogen bonding guided synthesis of ultrathin two-dimensional amorphous TiO₂ nanosheets. *Sci. China Mater.*, **2022**, 65 (11): 3017–3024.
- [18] Li Q W, Wang H, Tang X F, et al. Electrical conductivity adjustment for interface capacitive-like storage in sodium-ion battery. *Adv. Funct. Mater.*, **2021**, 31 (24): 2101081.
- [19] Han J, Hirata A, Du J, et al. Intercalation pseudocapacitance of amorphous titanium dioxide@nanoporous graphene for high-rate and large-capacity energy storage. *Nano Energy*, **2018**, 49: 354–362.
- [20] Lu C X, Li X Y, Liu R H, et al. Optimized Ti–O subcompounds and elastic expanded MXene interlayers boost quick sodium storage performance. *Adv. Funct. Mater.*, **2023**, 33 (19): 2215228.
- [21] Yang J P, Wang Y X, Li W, et al. Amorphous TiO₂ shells: A vital elastic buffering layer on silicon nanoparticles for high-performance and safe lithium storage. *Adv. Mater.*, **2017**, 29 (48): 1700523.
- [22] Ye J, Shea P, Baumgaertel A C, et al. Amorphization as a pathway to fast charging kinetics in atomic layer deposition-derived titania films for lithium ion batteries. *Chem. Mater.*, **2018**, 30 (24): 8871–8882.